Contrast Agents Hot Paper

DOI: 10.1002/ange.201404930

Phosphonated Near-Infrared Fluorophores for Biomedical Imaging of Bone**

*Hoon Hyun, Hideyuki Wada, Kai Bao, Julien Gravier, Yogesh Yadav, Matt Laramie, Maged Henary, John V. Frangioni, and Hak Soo Choi**

Abstract: *The conventional method for creating targeted contrast agents is to conjugate separate targeting and fluorophore domains. A new strategy is based on the incorporation of targeting moieties into the non-delocalized structure of pentamethine and heptamethine indocyanines. Using the known affinity of phosphonates for bone minerals in a model system, two families of bifunctional molecules that target bone without requiring a traditional bisphosphonate are synthesized. With peak fluorescence emissions at approximately 700 or 800 nm, these molecules can be used for fluorescence-assisted resection and exploration (FLARE) dual-channel imaging. Longitudinal FLARE studies in mice demonstrate that phosphonated near-infrared fluorophores remain stable in bone for over five weeks, and histological analysis confirms their incorporation into the bone matrix. Taken together, a new strategy for creating ultra-compact, targeted near-infrared fluorophores for various bioimaging applications is described.*

Near-infrared (NIR) fluorescence imaging of bone minerals, as first introduced in 2001,[1] required the covalent conjugation of a bisphosphonate or other bone-targeting ligand[2–4] to an NIR fluorophore, creating a bifunctional molecule for biomedical imaging.[4] Although preparative-scale synthesis,[5] hybrid optical/nuclear agents,[6] and various clinical applications[7,8] of these molecules were subsequently described, the basic chemical strategy remained unaltered.

However, the resonance properties of pentamethine and heptamethine indocyanines are not affected by a host of substituent modifications, which have little or no effect on the optical performance of the fluorophore.[2,3] We therefore hypothesized that several copies of a small substituent (ligand) that displays low affinities for a target tissue on its own could be incorporated into the polymethine cyanine core (a fluorophore) in such a way as to generate a final molecule with both high-affinity targeting and NIR fluorescence (i.e., a targeted contrast agent).[9–11] Herein, we explored this hypothesis by using the phosphonate group as the primary modification and also studied the ability of other substituents, such as sulfonates, to modify the performance of the final molecules.

As shown in Figure 1 a, four types of phosphonated NIR fluorophores were prepared from a pentamethine core for 700 nm fluorescence and a heptamethine core for 800 nm fluorescence, with the addition of sulfonates as indicated. The synthetic methods for P700 and P800 were slightly modified from the cGMP synthesis of ZW800-1, which was reported previously by our group.[12,13] Prior to measurement of optical properties and in vivo performance, each NIR fluorophore was purified to $\geq 95\,\%$ as measured using 210 nm absorbance (Supporting Information, Figure S1). The physicochemical and optical properties of all NIR fluorophores are summarized in Figure 1 b. By varying the side chains of the polymethine core, it was possible to systematically modify hydrophobicity, polarity, and electron-resonance properties without affecting the optical performance. Energy-minimized 3D structures showed similar distributions of charge and hydrophobicity over the molecular surface.

The specificity of these new NIR fluorophores for the biologically important calcium salts hydroxyapatite (HA), calcium carbonate (CC), calcium phosphate (CP), calcium oxalate (CO), and calcium pyrophosphate (CPP) was measured. As shown in Figure 2, all of the P700 and P800 fluorophores have a strong affinity for HA, but specificity was significantly different for molecules with additional sulfonates attached. In particular, a high affinity for CP, roughly equal to that for HA, was seen with P700SO3 and P800SO3, but not with P700H and P800H. Although the synergy of sulfonates with phosphonates for bone bonding is not well understood, sulfonate groups improve solubility in aqueous media and increase the ionization of hydroxy groups on the fluorophore because of strong electron-withdrawing effects.[14] One hypothesis is that two phenyl sulfonate groups bind a calcium ion by salt formation whereas the phosphonate group

[*] Dr. H. Hyun, Dr. H. Wada, Dr. K. Bao, Dr. J. Gravier, Dr. J. V. Frangioni, Dr. H. S. Choi
Division of Hematology/Oncology
Department of Medicine and Department of Radiology
Beth Israel Deaconess Medical Center
330 Brookline Avenue, SL436A, Boston, MA 02215 (USA)
E-mail: hchoi@bidmc.harvard.edu
Dr. Y. Yadav, Dr. M. Laramie, Dr. M. Henary
Department of Chemistry, Georgia State University
Atlanta, GA 30303 (USA)
Dr. J. V. Frangioni
Curadel, LLC
377 Plantation Street, Worcester, MA 01605 (USA)
Dr. H. S. Choi
Department of Cogno-Mechatronics Engineering
Pusan National University
Busan 609-735 (South Korea)

[**] This study was supported by the National Institutes of Health (NCI BRP grant R01-CA-115296 and NIBIB grants R01-EB-010022 and R01-EB-011523). We thank David Burrington, Jr. for help with the manuscript and Eugenia Trabucchi for administrative assistance. J.V.F. is currently CEO of Curadel, LLC, which has licensed FLARE imaging systems and contrast agents from the BIDMC.

Supporting information for this article is available on the WWW under http://dx.doi.org/10.1002/anie.201404930.

 © 2014 Wiley-VCH Verlag GmbH & Co. KGaA, Weinheim

a)

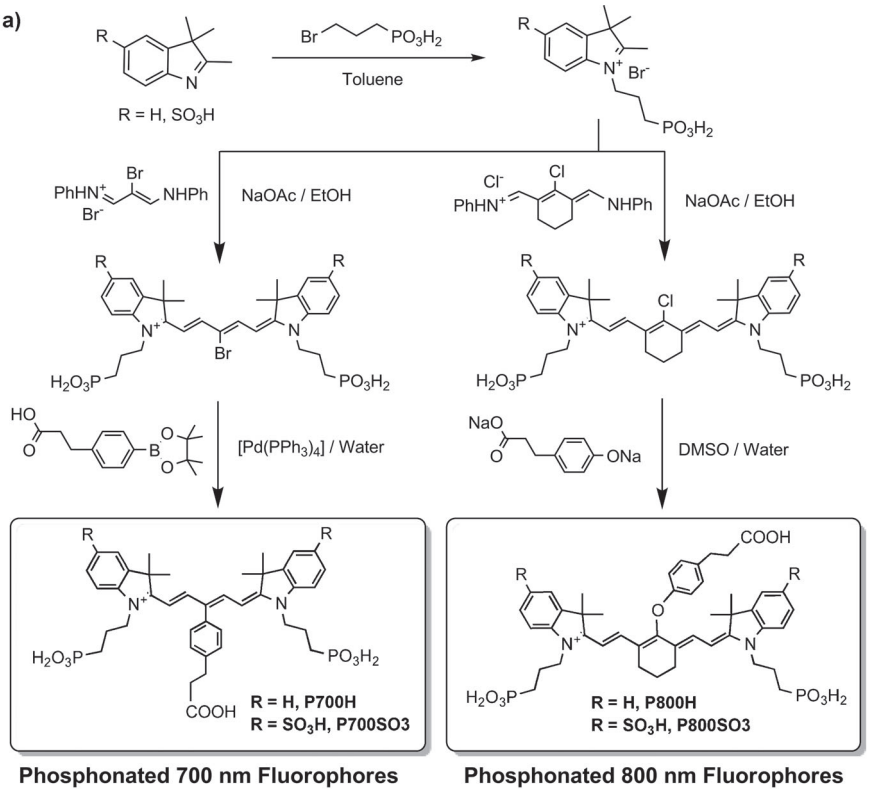

b)

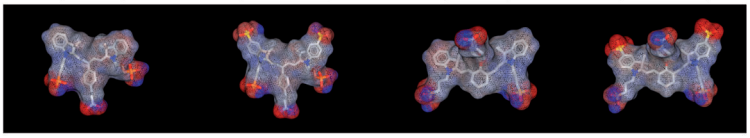

Property in **Serum**	P700H	P700SO3	P800H	P800SO3
Molecular Weight (Da)	746.77	904.88	828.87	986.98
Log *D* at pH 7.4 in silico	-0.27	-6.88	-0.42	-7.03
Total Polar Surface Area (Å^2)	161.44	275.84	170.67	285.07
Extinction Coefficient ($M^{-1}cm^{-1}$)	195000	179000	180000	210000
Absorbance Maximum (nm)	650	652	776	785
Emission Maximum (nm)	674	673	791	802
Stokes Shift (nm)	24	21	15	17
Quantum Yield (%)	28.9	23.1	14.4	15.1

Figure 1. a, b) Synthesis (a) and optical and physicochemical properties (b) of the P700 and P800 NIR fluorophores.

competes with serum phosphate ions and serves as a monodentate ligand for calcium binding.[15]

To explore bone targeting in vivo, phosphonated NIR fluorophores were administered intravenously into mice, and their biodistribution and clearance were measured over 4 and 24 hours. As shown in Figure 3a and 3b, P700H and P800H exhibited hepatic clearance from liver to the duodenum, whereas P700SO3 and P800SO3 were eliminated from the body by renal clearance into urine without nonspecific uptake by non-bone tissues and organs because of their low log *D* (distribution coefficient) values and high polarity.[12] At 24 hours post-injection, all P700 and P800 NIR fluorophores had been eliminated from the body, and only the bone signal was evident. Interestingly, P700SO3 and P800SO3 showed longer blood half-lives ($t_{1/2\beta}$; ca. 50 min) than P700H and P800H (26.6 min and 38.8 min, respectively; Table S1). These results highlight the effects of charge, hydrophobicity, and polarity of a targeted agent on its in vivo behavior.[12] As the bone targeting and biodistribution of P700SO3 and P800SO3 were most favorable, we selected these sulfonated fluorophores for further evaluation and optimization. To determine the dose of P700SO3 and P800SO3 that achieves the highest signal-to-background ratio (SBR), agents were intravenously administered in the range of 1 to 25 nmol and imaged at four hours post-injection. Although increasing the dose amplified the bone signal, there was diminishing return at higher doses because of increased background signal (Figure S2).

To confirm that these agents performed well across several species, particularly large animals with tissues and organs the size of humans, we injected 1 μmol (0.03 mg kg^{-1}) of P700SO3 and P800SO3 into 35 kg Yorkshire pigs. Both phosphonated NIR fluorophores resulted in intense signals for the bone at four hours post-injection with little nonspecific uptake by other tissues or organs (Figure 4), whereas commercially available BoneTag agents showed intense background signals for the skin, liver, and kidneys (Figure S3). The blood half-lives of P700SO3 and P800SO3 in pigs were 50.2 and 69.7 minutes, respectively, suggesting that an elimination period of 4–6 hours would be optimal in future human studies (Figure 4b).

We performed serial imaging of all NIR fluorophores in athymic nude mice over the course of five weeks. As shown in Figure 5a, the fluorescence signals of P700SO3 and P800SO3 were two times more intense than those of P700H and P800H. It is noteworthy that the SBR values for P700SO3 are lower than for P800SO3 because of skin autofluorescence in the 700 nm channel. Importantly, SBR values for the spine were stable over five weeks after a single intravenous injection (Figure S4). Magnified bone images of sacrificed and de-skinned mice at five weeks post-injection revealed exquisite imaging of bone tissue (Figure 5a). Microscopic analysis of cross-sectioned bones obtained at one day and five weeks post-injection revealed that P700SO3 and P800SO3 were stably incorporated into the bone matrix, with additional normal

 © 2014 Wiley-VCH Verlag GmbH & Co. KGaA, Weinheim

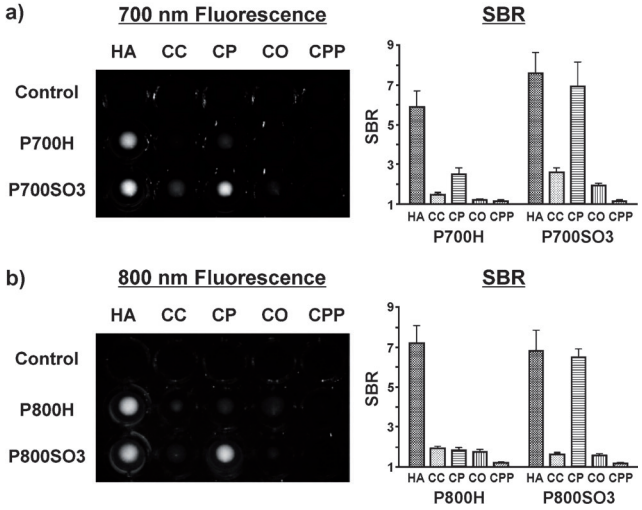

Figure 2. a, b) Calcium-salt binding properties of the P700 (a) and P800 (b) NIR fluorophores. SBR was calculated by dividing the fluorescence intensity of each fluorophore sample by the signal intensity of each control sample. All of the NIR fluorescence images have identical exposure and normalizations. Images are representative of $n = 3$ independent experiments. CC = calcium carbonate, CO = calcium oxalate, CP = calcium phosphate, CPP = calcium pyrophosphate, HA = hydroxyapatite.

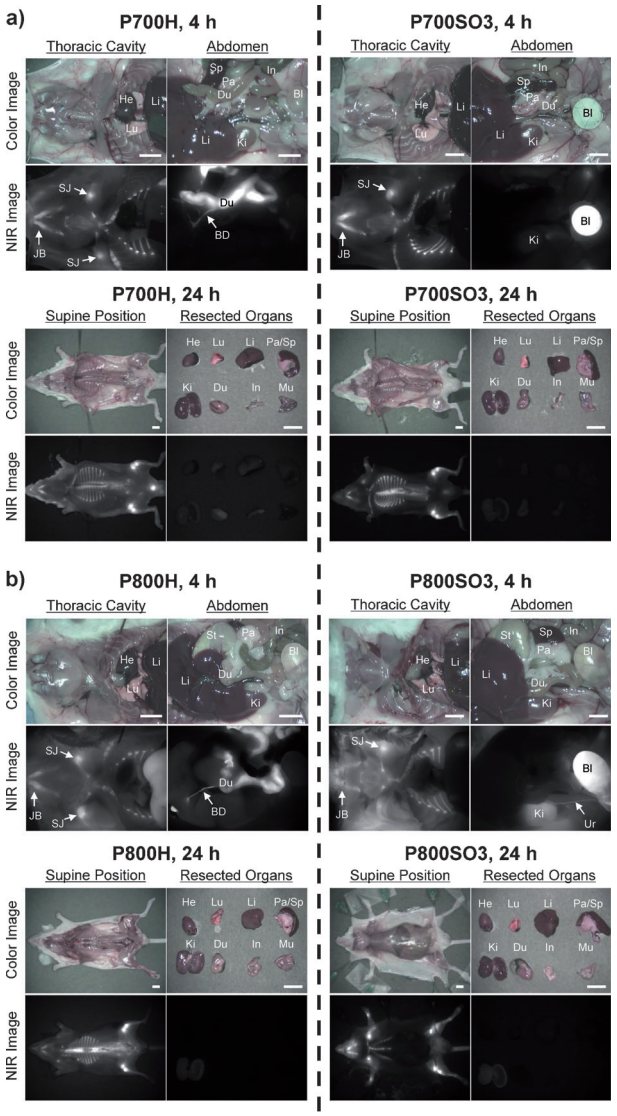

Figure 3. a, b) In vivo biodistribution and bone tissue imaging using the P700 (a) and P800 (b) NIR phosphonates in mice. Each NIR fluorophore was intravenously injected into 20 g CD-1 or athymic nude mice (10 nmol; 0.4 mg kg^{-1}) 4 and 24 hours prior to imaging. Scale bars = 1 cm. Images are representative of $n = 3$ independent experiments. BD = bile duct, Bl = bladder, Du = duodenum, He = heart, In = intestine, JB = jaw bone, Ki = kidneys, Li = liver, Lu = lungs, Mu = muscle, Pa = pancreas, SJ = shoulder joint, Sp = spleen, St = stomach, Ur = ureter.

bone matrix deposited on top of the NIR fluorophores over time (Figure 5b).

In this study, we hypothesized that chemical substituents with low affinity for a target tissue could be incorporated into the non-delocalized backbone of an NIR fluorophore to create a new contrast agent with high affinity.[16] Based on the results, this strategy appears to work well, at least with the phosphonate model system. We did, however, see significant modulation of the contrast-agent performance from additional side groups. The addition of sulfonate groups improved biodistribution and clearance, resulting in a more intense signal, lower background radiation, and improved elimination of unbound fluorophores from the body.

The improvement in SBR through sulfonation, however, came at the price of specificity. P700H and P800H bind calcium salts in a fashion that is most similar to that of a conventional bisphosphonate conjugated to a NIR fluorophore,[1,5,17,18] i.e., high HA specificity. However, P700SO3 and P800SO3 exhibited strong binding to CP as well as HA. For in vivo imaging of bone and urinary crystals,[8,19] CP binding might actually be an advantage, because otherwise, binding would be restricted to sites of osteoblastic activity. However, if HA specificity is the goal, then a conventional bisphosphonate–NIR fluorophore conjugate will be most suitable.

Importantly, the new molecules that are described in this study appear to be stably incorporated into the bone matrix without interfering with normal bone deposition (Figure 5b). In fact, NIR fluorescence of bone remained intact and stable for at least five weeks post-injection. This long-term stability could be ideal for tissue engineering experiments where neo-ossification needs to be followed for days and months. For studies of drugs that modulate either osteoblast or osteoclast activity, long-acting contrast agents would permit quantitative, ratiometric imaging of bone growth and resorption of minerals over time.

Finally, we purposely engineered a single carboxylic acid into each molecule, which permits conjugation to other functional molecules and therapeutics. For example, this chemical group could be used to attach drugs that modulate osteoblasts or osteoclasts or diagnostic or therapeutic radioisotopes, creating trifunctional theranostic agents. Furthermore, non-hormonal phosphonates increase bone strength, and repeated injections of this theranostic agent will improve bone density by preventing the loss of minerals.

© 2014 Wiley-VCH Verlag GmbH & Co. KGaA, Weinheim

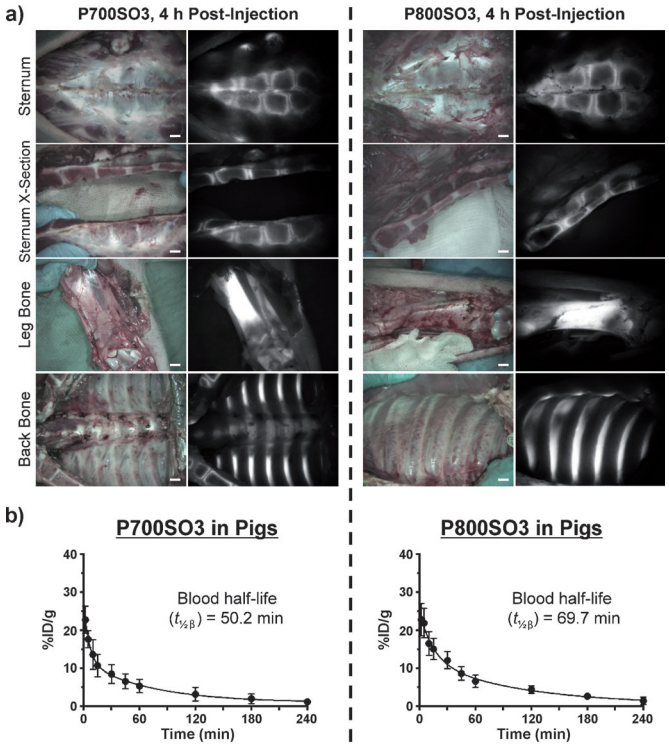

Figure 4. In vivo biodistribution and bone tissue imaging using the NIR phosphonates P700SO3 and P800SO3 in pigs. a) 30 pmol g^{-1} of P700SO3 and P800SO3 were intravenously injected into 35 kg Yorkshire pigs four hours prior to imaging. b) Blood clearance (% ID/g) and blood half-life (mean ± 95% confidence intervals) of P700SO3 and P800SO3 in pigs. All NIR fluorescence images were recorded with the same exposure times and normalizations. Scale bars = 1 cm. Images are representative of $n = 3$ independent experiments.

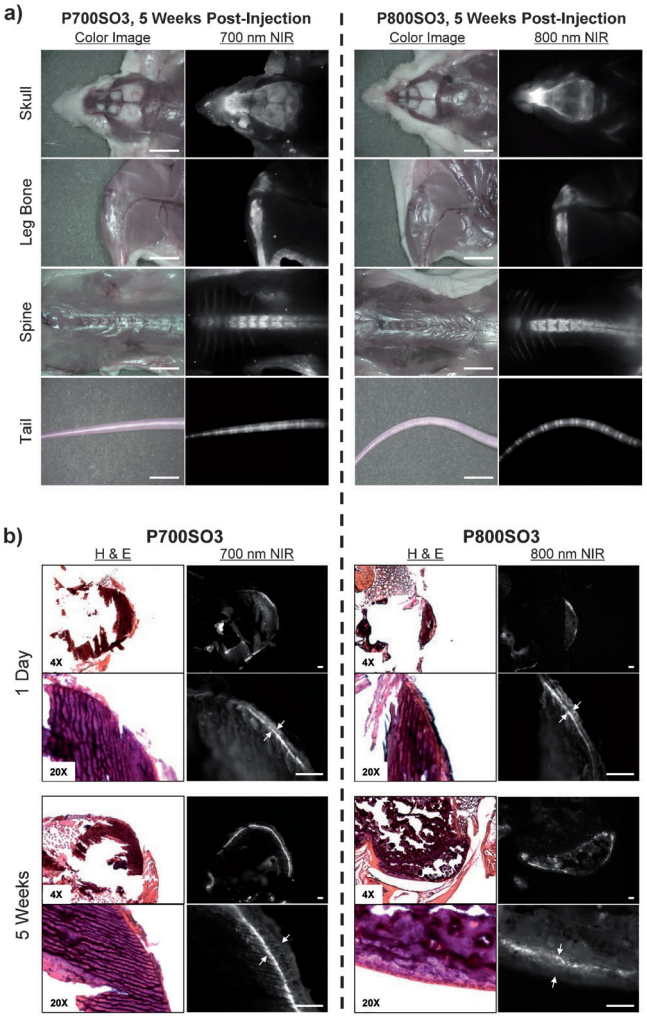

Figure 5. Stable incorporation of phosphonated NIR fluorophores into bone matrix. a) P700SO3 and P800SO3 were injected intravenously into 20 g athymic nude mice (10 nmol, 0.4 mg kg^{-1}) five weeks prior to imaging. Scale bars = 1 cm. b) H&E and NIR imaging of resected bone tissues at one day and five weeks post-injection of P700SO3 and P800SO3. Scale bars = 100 μm. All NIR fluorescence images for each set of conditions were recorded with the same exposure times and normalizations.

Experimental Section

Synthesis of P700 and P800 NIR fluorophores: All chemicals and solvents were of American Chemical Society grade or HPLC purity. Starting materials were purchased from Sigma–Aldrich (Saint Louis, MO) and Fisher Scientific Inc. (Pittsburgh, PA) and used without purification. Final products were separated by a preparative HPLC system (Waters, Milford, MA, USA) equipped with a PrepLC 150 mL fluid handling unit, a manual injector (Rheodyne 7725i), a 2487 dual-wavelength absorbance detector (Waters), and an evaporative light-scattering detector (ELSD, Richards Scientific, Novato, CA, USA). See the Supporting Information for detailed chemical syntheses and analyses.

NIR fluorescence imaging system: The dual-NIR channel FLARE imaging system has previously been described in detail.[20–22] Herein, 670 nm excitation light (4 mW cm^{-2}) and 760 nm excitation light (11 mW cm^{-2}) were used with white light (400–650 nm) at 40000 lx. Color and NIR fluorescence images were acquired simultaneously with custom software at rates of up to 15 Hz over a field of view with a diameter of 15 cm. The imaging system was positioned at a distance of 46 cm from the surgical field. For each experiment, camera exposure time and image normalization were held constant.

Quantitative analysis: At each time point, the fluorescence and background intensities of a region of interest (ROI) over each tissue were quantified using custom FLARE software. The signal-to-background ratio (SBR) was calculated as SBR = fluorescence/background, where background is the signal intensity of neighboring tissues, such as muscle or skin, obtained over the imaging period. All NIR fluorescence images for a particular fluorophore were normalized identically for all conditions of an experiment. At least three animals were analyzed at each time point. Statistical analysis was carried out using the unpaired Student's *t*-test or one-way analysis of variance (ANOVA). Results are presented as mean ± standard deviation, and curve fitting was performed using the Prism version 4.0a software (GraphPad, San Diego, CA).

Histology and NIR fluorescence microscopy: Bone tissues were placed in 2% paraformaldehyde solutions in phosphate-buffered saline (PBS) for 30 minutes before mounting in Tissue-Tek OCT compound (Fisher Scientific, Pittsburgh, PA) and flash-freezing in liquid nitrogen. Frozen samples were cryosectioned (10 μm per slice), analyzed by NIR fluorescence microscopy, and also stained with hematoxylin and eosin (H&E). NIR fluorescence microscopy was performed on a 4-filter Nikon Eclipse TE300 microscope system as previously described.[9,23,24] The microscope was equipped with a 100 W mercury light source (Chiu Technical Corporation, Kings Park, NY), NIR-compatible optics, and a NIR-compatible 10X Plan Fluor objective lens and a 100X Plan Apo oil immersion objective lens (Nikon, Melville, NY). Images were acquired on an Orca-AG

© 2014 Wiley-VCH Verlag GmbH & Co. KGaA, Weinheim

apparatus (Hamamatsu, Bridgewater, NJ). Image acquisition and analysis was performed using iVision software (BioVision Technologies, Exton, PA). Two custom filter sets (Chroma Technology Corporation, Brattleboro, VT) with 650 ± 22 nm and 750 ± 25 nm excitation filters, 675 nm and 785 nm dichroic mirrors, and 710 ± 25 nm and 810 ± 20 nm emission filters were respectively used to detect P700SO3 and P800SO3 signals in the frozen tissue samples.

Received: May 7, 2014
Published online: August 19, 2014

Keywords: fluorophores · imaging agents · medicinal chemistry · near-infrared fluorescence

[1] A. Zaheer, R. E. Lenkinski, A. Mahmood, A. G. Jones, L. C. Cantley, J. V. Frangioni, *Nat. Biotechnol.* **2001**, *19*, 1148 – 1154.
[2] J. L. Kovar, X. Xu, D. Draney, A. Cupp, M. A. Simpson, D. M. Olive, *Anal. Biochem.* **2011**, *416*, 167 – 173.
[3] C. Pautke, S. Vogt, K. Kreutzer, C. Haczek, G. Wexel, A. Kolk, A. B. Imhoff, H. Zitzelsberger, S. Milz, T. Tischer, *J. Anat.* **2010**, *217*, 76 – 82.
[4] E. A. Cowles, J. L. Kovar, E. T. Curtis, H. Xu, S. F. Othman, *BioRes. Open Access* **2013**, *2*, 186 – 191.
[5] K. R. Bhushan, E. Tanaka, J. V. Frangioni, *Angew. Chem.* **2007**, *119*, 8115 – 8117; *Angew. Chem. Int. Ed.* **2007**, *46*, 7969 – 7971.
[6] K. R. Bhushan, P. Misra, F. Liu, S. Mathur, R. E. Lenkinski, J. V. Frangioni, *J. Am. Chem. Soc.* **2008**, *130*, 17648 – 17649.
[7] A. Zaheer, M. Murshed, A. M. De Grand, T. G. Morgan, G. Karsenty, J. V. Frangioni, *Arterioscler. Thromb. Vasc. Biol.* **2006**, *26*, 1132 – 1136.
[8] E. Aikawa, M. Nahrendorf, J. L. Figueiredo, F. K. Swirski, T. Shtatland, R. H. Kohler, F. A. Jaffer, M. Aikawa, R. Weissleder, *Circulation* **2007**, *116*, 2841 – 2850.
[9] H. S. Choi, S. L. Gibbs-Strauss, J. H. Lee, S. H. Kim, Y. Ashitate, F. Liu, H. Hyun, G. Park, Y. Xie, S. Bae, M. Henary, J. V. Frangioni, *Nat. Biotechnol.* **2013**, *31*, 148 – 153.
[10] Y. Ashitate, H. Hyun, S. H. Kim, J. H. Lee, M. Henary, J. V. Frangioni, H. S. Choi, *Theranostics* **2014**, *4*, 693 – 700.
[11] M. H. Park, H. Hyun, Y. Ashitate, H. Wada, G. Park, J. H. Lee, C. Njiojob, M. Henary, J. V. Frangioni, H. S. Choi, *Theranostics* **2014**, *4*, 823 – 833.
[12] H. S. Choi, K. Nasr, S. Alyabyev, D. Feith, J. H. Lee, S. H. Kim, Y. Ashitate, H. Hyun, G. Patonay, L. Strekowski, M. Henary, J. V. Frangioni, *Angew. Chem.* **2011**, *123*, 6382 – 6387; *Angew. Chem. Int. Ed.* **2011**, *50*, 6258 – 6263.
[13] H. Hyun, M. W. Bordo, K. Nasr, D. Feith, J. H. Lee, S. H. Kim, Y. Ashitate, L. A. Moffitt, M. Rosenberg, M. Henary, H. S. Choi, J. V. Frangioni, *Contrast Media Mol. Imaging* **2012**, *7*, 516 – 524.
[14] A. Mozar, N. Haren, M. Chasseraud, L. Louvet, C. Maziere, A. Wattel, R. Mentaverri, P. Morliere, S. Kamel, M. Brazier, J. C. Maziere, Z. A. Massy, *J. Cell. Physiol.* **2008**, *215*, 47 – 54.
[15] T. Moriguchi, K. Yano, S. Nakagawa, F. Kaji, *J. Colloid Interface Sci.* **2003**, *260*, 19 – 25.
[16] H. Hyun, M. H. Park, E. A. Owens, H. Wada, M. Henary, H. J. M. Handgraaf, A. L. Vahrmeijer, J. V. Frangioni, H. S. Choi, *Nat. Med.* **2014**, in press.
[17] K. M. Harmatys, E. L. Cole, B. D. Smith, *Mol. Pharmaceutics* **2013**, *10*, 4263 – 4271.
[18] H. Nakayama, T. Kawase, K. Okuda, L. F. Wolff, H. Yoshie, *Acta Radiol.* **2011**, *52*, 978 – 988.
[19] K. M. Kozloff, R. Weissleder, U. Mahmood, *J. Bone Miner. Res.* **2007**, *22*, 1208 – 1216.
[20] S. L. Troyan, V. Kianzad, S. L. Gibbs-Strauss, S. Gioux, A. Matsui, R. Oketokoun, L. Ngo, A. Khamene, F. Azar, J. V. Frangioni, *Ann. Surg. Oncol.* **2009**, *16*, 2943 – 2952.
[21] Y. Ashitate, S. H. Kim, E. Tanaka, M. Henary, H. S. Choi, J. V. Frangioni, R. Flaumenhaft, *J. Vasc. Surg.* **2012**, *56*, 171 – 180.
[22] S. Gioux, H. S. Choi, J. V. Frangioni, *Mol. Imaging* **2010**, *9*, 237 – 255.
[23] H. S. Choi, Y. Ashitate, J. H. Lee, S. H. Kim, A. Matsui, N. Insin, M. G. Bawendi, M. Semmler-Behnke, J. V. Frangioni, A. Tsuda, *Nat. Biotechnol.* **2010**, *28*, 1300 – 1303.
[24] H. S. Choi, B. I. Ipe, P. Misra, J. H. Lee, M. G. Bawendi, J. V. Frangioni, *Nano Lett.* **2009**, *9*, 2354 – 2359.

© 2014 Wiley-VCH Verlag GmbH & Co. KGaA, Weinheim